Master Thesis

2010

A Study on Electrical and Magnetic Characterization of $Co_{87}Zr_5Nb_8$ Films for High-Q On-chip Inductors

Supervisor

Professor Nobuyuki Sugii

Professor Hiroshi Iwai

Department of Electronics and Applied Physics

Interdisciplinary Graduate School of Science and Engineering

Tokyo Institute of Technology

08M53403

Mokh. Sholihul Hadi

CONTENTS

Chapter 1
Introduction

1.1 Background of This Study

1.2 On-chip inductor

1.3 Soft Magnetic Material

1.4 Objective of this study

1.1 Background of This Study

In recent years, power supply voltage for LSIs has been decreasing year after year, as the result of CMOS downscaling. The power supply voltage is now primarily at 0.9 – 1.2 V in the logic circuits. On the other hand, the supply voltage from a rechargeable lithium-ion battery of 3.6 V is mainly used for portable electronic equipments. Due to the increase of difference between the battery voltage and LSI operating voltage, high-efficiency voltage converter with reduced power loss have come to attract widespread attention. So far, it has been investigated that series regulator are replaced with switching dc–dc converters in many systems, because the dc–dc converter has great advantage of efficiency in high conversion ratio. But the conventional dc–dc converters are larger in size than the series regulators. Therefore it is required to reduce their size and thickness.

In order to shrink the size, the dc-dc converter should operate at higher frequencies because passive elements can be smaller. Therefore, a technology to fabricate passive elements that can be operated at high frequencies is urgently needed. Most of dc-dc converters usually operate at

frequencies in the range of 100 kHz to 500 kHz, which are not suitable for further reduction of the sizes of passive elements. High-Q on-chip inductor has been a major challenge in the move towards in integrating the on-chip dc-dc converter with high efficiency in a LSI chip. Most of on-chip inductors in the literatures use a spiral geometry fabricated without magnetic material and exhibit inductances ranging from 1 to 10 nH, but consume large amount of area [5]. With the addition of magnetic material, increased inductance L and quality factor Q with decreased capacitance, resistance, and area can be achieved [1, 2, 4].

The on-chip inductor with magnetic material is needed to shrink its dimension and to increase the inductance. The inductance however drops at frequencies >100 MHz due to eddy currents circulating in the magnetic film that generate resistive loss [1]. Considering a trade off between dimension and inductance, a switching frequency range of 100 MHz to 500 MHz will be suited. One of the important properties of the magnetic thin films required for such applications is their high-frequency properties. The $Co_{87}Zr_5Nb_8$ amorphous film has been considered as a candidate material because amorphous magnetic material allows smaller, lighter and more

energy efficient designs in many high frequency applications compared to nano-crystalline materials [3]. The coercivity and saturation magnetization of the magnetic material are also important factors because they determine the hysteretic loss and maximum eddy current.

1.2 On chip inductor

The on-chip inductors are commonly used for filter, amplifier, or resonant circuits used in radio-frequency applications. The inductance have typical values ranging from 1 to 100 nH, which give an equivalent impedance between 10 and 1000 Ω, within the radio-frequency range at 300 MHz - 3 GHz (Figure 1.1). At frequencies lower than 100 kHz, discrete inductors are used because of their high inductance values (From 1 to 100 μH) to keep the impedance between 10 and 1000 Ω. Such high inductances cannot be integrated in a reasonable silicon area. Around 1 GHz, a 10 nH on-chip inductor matches the standard 50 Ω impedance of most input and output stages in very high frequency applications.

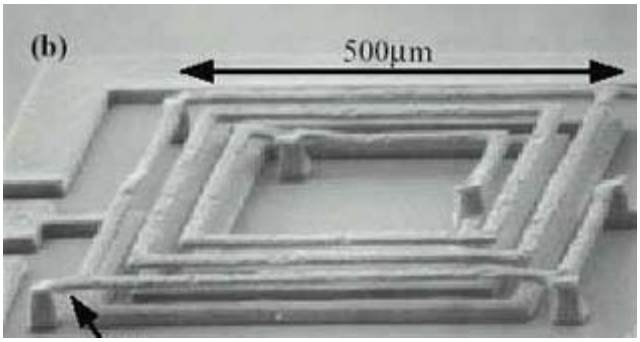

Figure 1-1. On-chip inductor with square model [14]

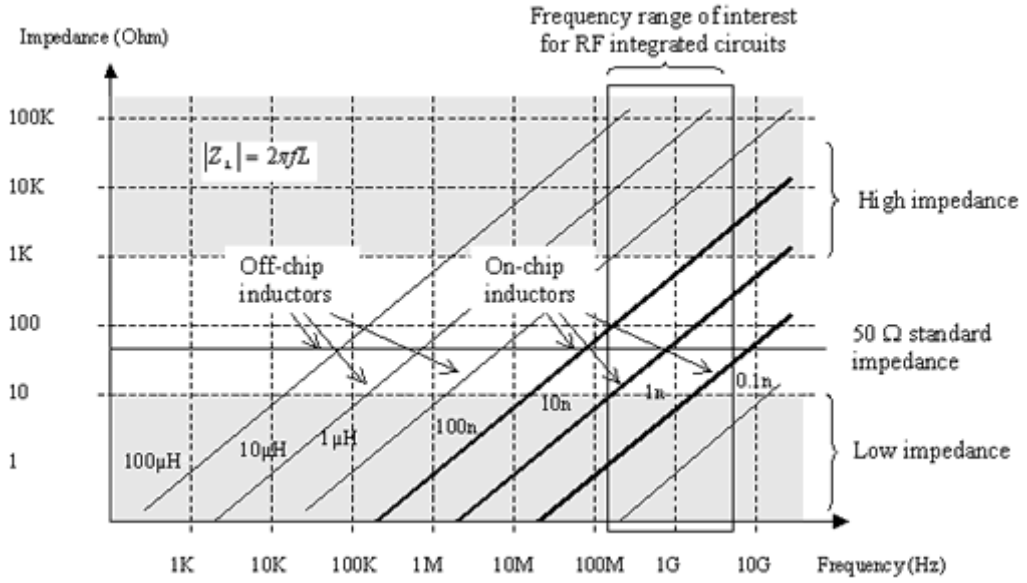

Figure 1-2. The inductor impedance versus frequency [14]

1.3 Soft Magnetic Material

Soft magnetic materials are essential constituents of nearly every electrical device of modern civilization. So named because of the correlation in ordinary steels between mechanical softness and ease of magnetization reversal, soft magnetic materials perform the crucial task of

concentrating and shaping magnetic flux. The continuous development to obtain better materials has resulted both in improved efficiencies of key building blocks of present technologies: motors, generators, transformers, inductors, and sensors in novel devices and applications.

It is widely recognized that most of the important properties for a magnetic design engineer arise from a complex interplay between fundamental properties controlled at the atomic level and the complex and sophisticated processing used in the modern materials industry. "Enlightened empiricism,"in the phrase of Gifkins, has been achieved inspiration.

In this light, the development of soft magnetic materials has been driven by the needs of design engineers. From the early days of this century, research has been focused on simply stated goals: the desire for higher permeability ρ, saturation induction σ, lower coercivity H_c, and core loss. Improvements in these properties have resulted in power-handling electrical devices with reduced size and weight and increased efficiency.

1.4 Objective of this study

This research presents a study on electrical and magnetic characterization of $Co_{87}Zr_5Nb_8$ films, which represent one of the desirable promising amorphous magnetic material for proposed frequency range. The magnetic material should have minimal hysteresis loss, high saturation magnetization, low magnetostriction, high resistivity, and compatible with Si technology.

Chapter 2

Fabrication and Characterization Method

2.1 Experimental Procedure

2.1.1 Si Substrate Cleaning Process

2.1.2 Facing Target Sputtering

2.2 Measurement Methods

2.2.1 Scanning Electron Microscope (SEM)

2.2.2 Four-Point Probe Technique

2.2.3 Permeameter

2.2.4 Vibrating Sample Magnetometer

2.1 Experimental Procedure

2.1.1 Si Substrate Cleaning Process

At first, high quality thin films require ultra clean Si surface without particle contamination, metal contamination, organic contamination, ionic contamination, water absorption, native oxide and atomic scale roughness.

One of the most important chemicals used in Si substrate cleaning is DI (de-ionized) water. DI water is highly purified and filtered to remove all traces of ionic, particulate, and bacterial contamination. The theoretical resistivity of pure water is 18.25 MΩcm at 25^{o}C. Ultra-pure water (UPW) system used in this study provided UPW of more than 18.2 MΩcm at resistivity, fewer than 1 colony of bacteria per milliliter and fewer than 1 particle per milliliter.

In this study, the Si substrate was cleaned on a basis of RCA cleaning process. The first step, which uses a mixture of sulfuric acid (H_2SO_4) / hydrogen peroxide (H_2O_2) (H_2SO_4: H_2O_2=4:1), was performed to remove any organic material and metallic impurities. After that, the native or chemical oxide was removed by diluted hydrofluoric acid (HF:H_2O=1:99). Then the cleaned wafer was dipped in DI water. Finally, the cleaned Si

substrate was loaded to the deposition chamber just after it was dried by air gun.

2.1.2 Facing Target Sputtering

The amorphous $Co_{87}Zr_5Nb_8$ alloy films were deposited on Si wafers covered with a 400-nm thick SiO_2 layer using a facing-target sputtering apparatus at room temperature, resulting the introduction of in-plane magnetic anisotropy, hard axis and easy Axis of magnetization, as shown in Fig 2.1. Before the deposition, the chamber was evacuated to less than 8 x 10^{-7} Torr, and during the sputter deposition, the chamber was maintained at 0.25 mTorr, 0.5 mTorr, 0.75 mTorr, or 1 mTorr, using argon gas. A dc bias of 50 V was applied to the substrate during the deposition. An external magnetic field of ~35 Oe was applied to the substrates with permanent magnets placed behind the facing targets. Figure 2.2 shows the facing target sputtering apparatus chamber. Figure 2.3 shows the schematic drawing of FTS vacuum chamber.

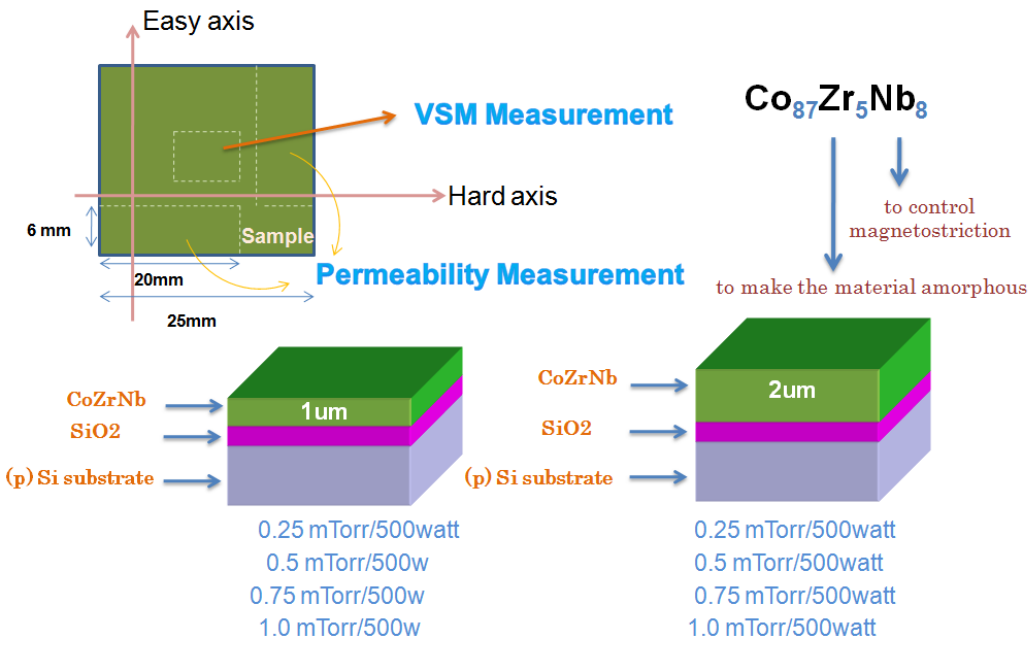

Figure 2.1. Fabrication and characterization of CoZrNb films

Figure 2.2. Facing Target Sputtering apparatus chamber

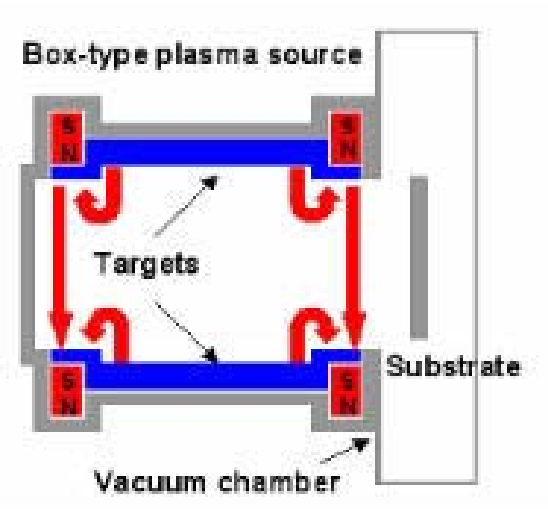

Figure 2.3.Schematic drawing of FTS vacuum chamber

2.2 Measurement Methods

2.2.1 Scanning Electron Microscope (SEM)

Figure 2.4 shows Scanning Electron Microscope (SEM) system. The equipment is S-4800 (HITACHI High-Technologies Corporation). Schematic drawing of electron beam system is shown in Fig. 2.5. The 'Virtual Source' at the top represents the electron gun, producing a stream of monochromatic electrons. The stream is condensed by the first condenser lens. This lens is used to both form the beam and limit the amount of current in the beam. It works in conjunction with the condenser aperture to eliminate the high-angle electrons into a thin, tight, coherent beam. A user selectable objective aperture further eliminates high-angle

electrons from the beam. A set of coils then scan or sweep the beam in a grid fashion and make the beam dwell on points for a period of time determined by the scan speed. The final lens, the Objective, focuses the scanning beam onto the part of the specimen desired. When the beam strikes the sample, interactions occur inside the sample and are detected with various instruments interactions. Before the beam moves to its next dwell point these instruments count the number of interactions and display a pixel on a CRT whose intensity is determined by this number. This process is repeated until the grid scan is finished and then repeated, the entire pattern can be scanned 30 times per second.

Figure 2.4 Photograph of SEM equipment.

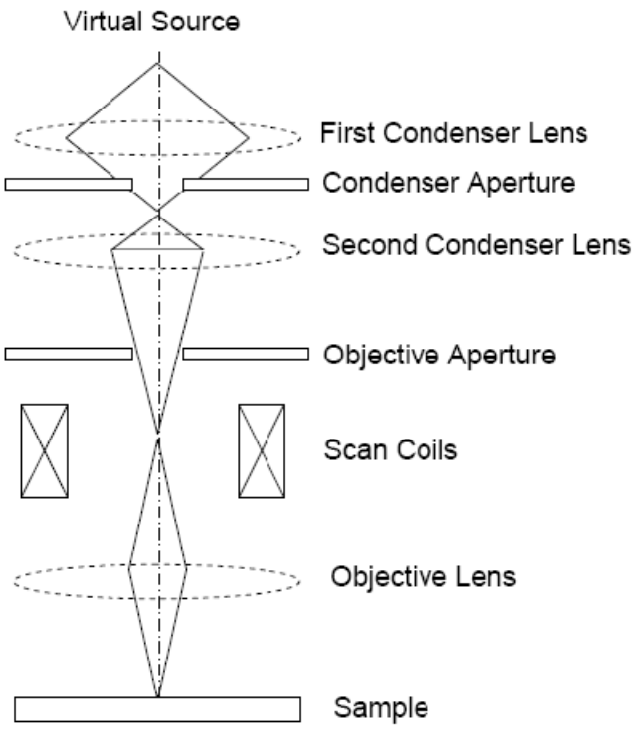

Figure 2.5 Schematic drawings of SEM equipment.

2.2.2 Four-Point Probe Technique

The electrical resistivity was measured by using a conventional four probe method. The four-point probe technique is one of the most common methods for measuring the semiconductor resistivity because the measured value by two-point probe includes parasitic effects. The sheet resistance is calculated from potential difference between inside 2 terminals (between B probe and C probe) after applying the current between outside

2 terminals (between A probe and D probe) as shown in fig. 2.5. The resistance by two-probe technique is higher than accurate resistance because it includes the contact resistance (R**C**) between metal probe and semiconductor surface and spreading resistance (R**SP**) of each probe. Neither RC nor RSP can be accurately calculated and thus semiconductor resistance (R**S**) cannot be accurately extracted from the measured resistance. On the other hand, four-probe technique can neglect these parasitic resistances because the current which flows between the voltage terminals is very small and potential drop can be disregarded. In this study, sheet resistance was measured by four-probe technique. For an arbitrarily shaped sample the sheet resistance (ρ***sh***) is given by

$$\rho_{sh} = V / I * CF \qquad (2.1)$$

where CF is correction factor that depends on the sample geometry. If the distance among probes (s; in this study, s=1 mm) is greatly shorter than the width of a sample (d), CF equals to $\pi/\ln(2)=4.5$

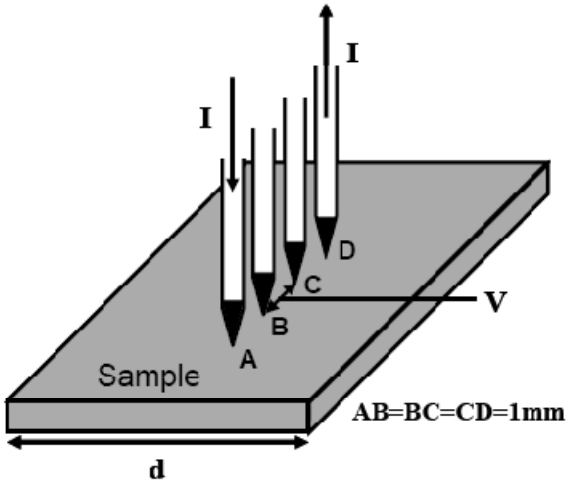

Fig 2.6. Illustration of four point probe system

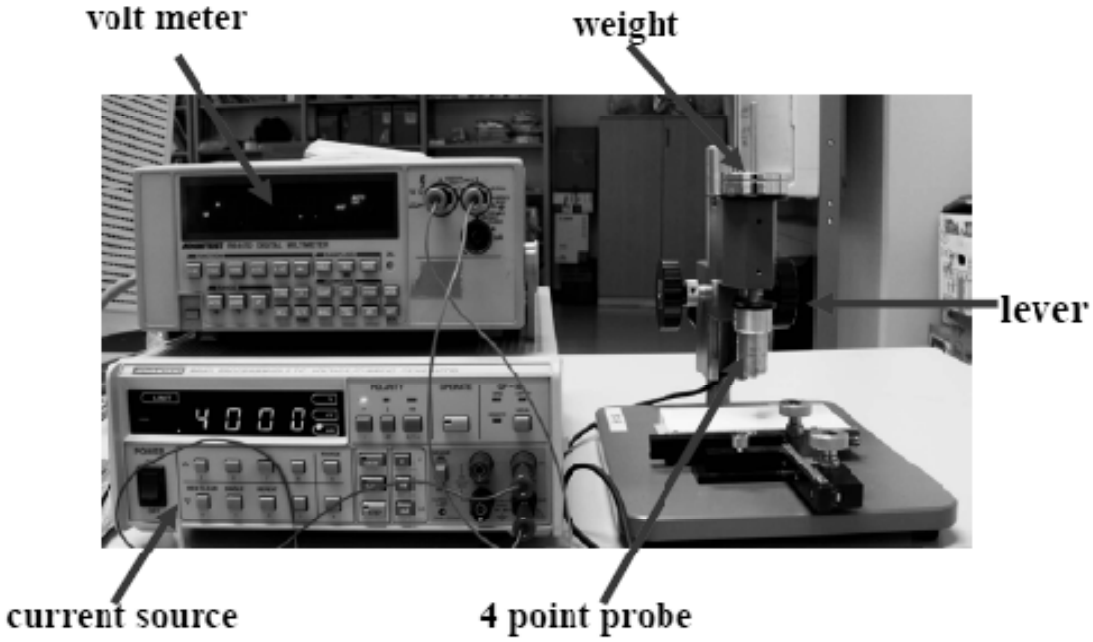

Fig 2.7. Photograph of four point probe system

2.2.3 Permeameter

The hard-axis magnetic permeability was measured by using a permeance meter with a frequency range from 1 MHz to 3 GHz. The principle work of permeameter can be explained as follows, two electrical inductors formed as primary and secondary concentric coils share a common magnetic core space. An ac voltage applied to the primary coil creates a magnetic flux in the core proportional to the magnetic permeability of a sample of the material positioned within the core space. The magnetic flux induces an ac voltage in the secondary coil indicative of the sample magnetic permeability. When the material is a magnetorheological fluid, the magnetic permeability is proportional to the concentration of magnetic particles in the sample and can be back-calculated from the amplitude of the secondary voltage signal. Sensitivity and resolution can be increased by using two identical sets of coils wherein a reference material forms a core for the primary set and the MR fluid sample forms a core for the secondary set. Figure 2.8 shows permeameter apparatus. Figure 2.9 shows the schematic drawings of permeameter apparatus.

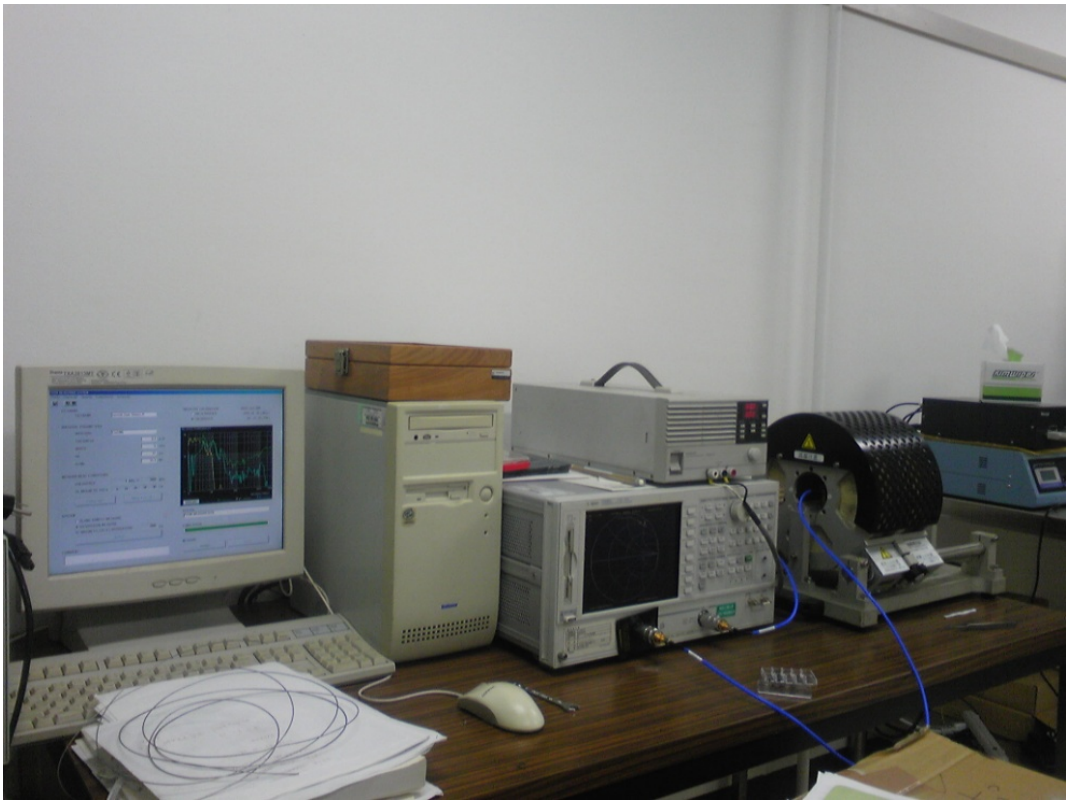

Fig 2.8. Photograph of permeameter

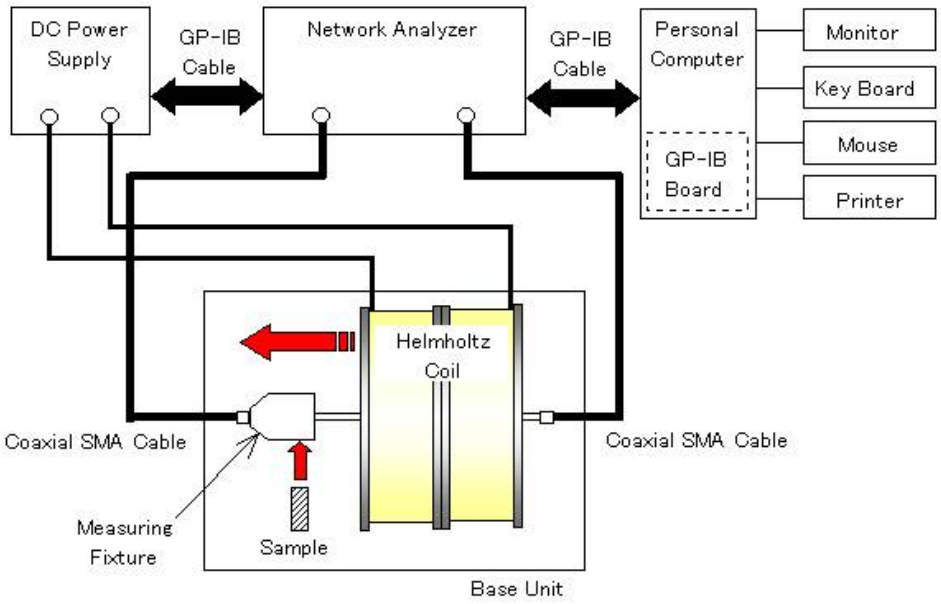

Figure 2.9 Schematic drawings of permeameter.

2.2.4 Vibrating Sample Magnetometer

Magnetic measurements of the films were performed with a vibrating sample magnetometer (VSM) at room temperature. A sample is placed inside a uniform magnetic field to magnetize the sample. The sample is then physically vibrated sinusoidally, typically through the use of a piezoelectric material. Commercial systems use linear attenuators of some form and historically the development of these systems was done using modified audio speakers, though this approached was dropped due to the interference through the in-phase magnetic noise produced, as the magnetic flux through a nearby pickup coil varies sinusoidally. The induced voltage in the pickup coil is proportional to the sample's magnetic moment, but does not depend on the strength of the applied magnetic field. In a typical setup, the induced voltage is measured through the use of a lock-in amplifier using the piezoelectric signal as its reference signal. By measuring in the field of an external electromagnet, it is possible to obtain the hysteresis curve of a material.

If a sample of any material is placed in a uniform magnetic field, created between the poles of a electromagnet, a dipole moment will be

induced. If the sample vibrates with sinusoidal motion a sinusoidal electrical signal can be induced in suitable placed pick-up coils. The signal has the same frequency of vibration and its amplitude will be proportional to the magnetic moment, amplitude, and relative position with respect to the pick-up coils system. Fig. 2.8 shows the vibrating sample magnetometer block diagram.

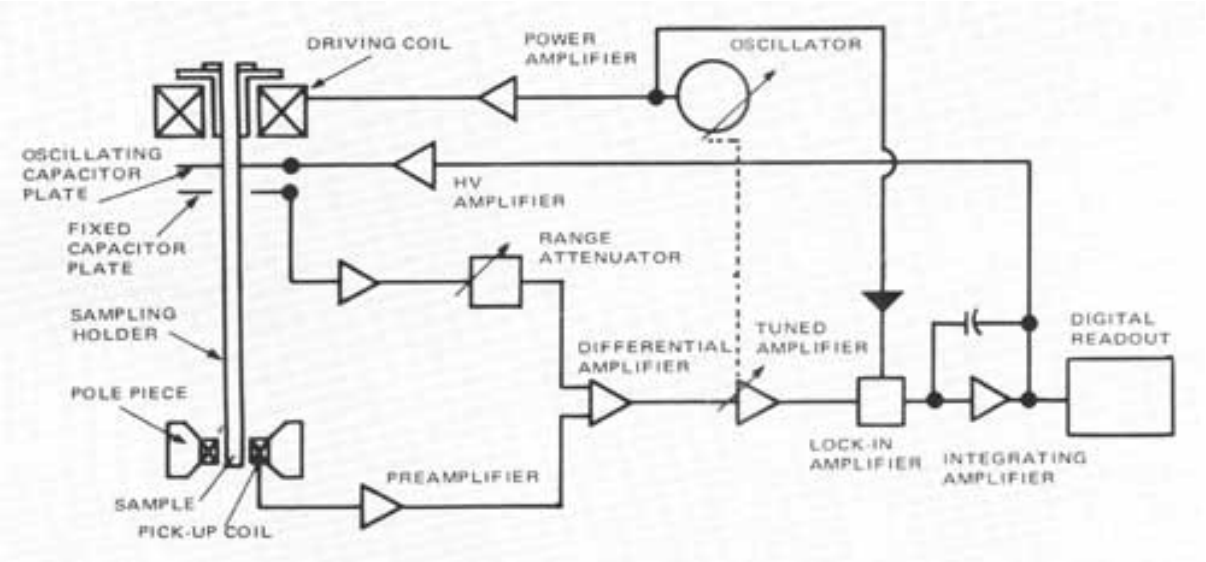

Fig. 2.8 Vibrating sample magnetometer block diagram.

The sample is fixed to a small sample holder located at the end of a sample rod mounted in a electromechanical transducer. The transducer is driven by a power amplifier which itself is driven by an oscillator at a frequency of 90 Hertz. So, the sample vibrates along the Z axis perpendicular to the

magnetizing field. The latter induced a signal in the pick-up coil system that is fed to a differential amplifier. The output of the differential amplifier is subsequently fed into a tuned amplifier and an internal lock-in amplifier that receives a reference signal supplied by the oscillator. The output of this lock-in amplifier, or the output of the magnetometer itself, is a dc signal proportional to the magnetic moment of the sample being studied. The electromechanical transducer can move along X, Y and Z directions in order to find the saddle point (which Calibration of the vibrating sample magnetometer is done by measuring the signal of a pure Ni standard of known the saturation magnetic moment placed in the saddle point.

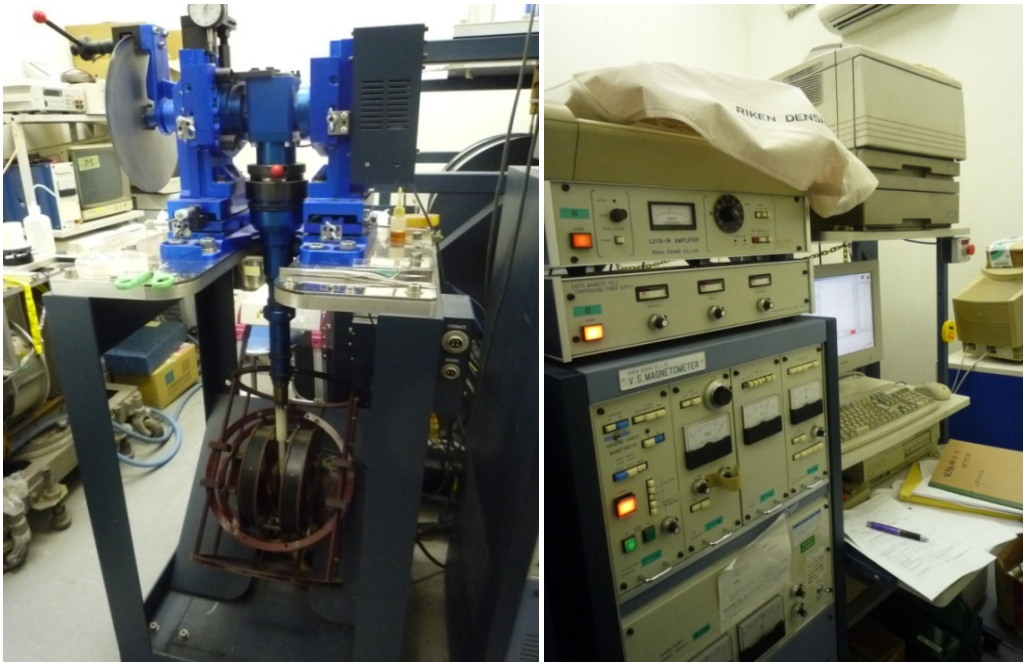

Fig 2.9. Photograph of vibrating sample magnetometer

Chapter 3
BASIC MAGNETIC CONSIDERATIONS OF SOFT MAGNETIC MATERIAL

3.1. B-H Loop Shape

3.2 Core Loss

3.3 Magnetic Anisotropy

3.4 Coercivity Field

3.5 Domain wall

3.6 Magnetostriction

3.7 Permeability

3.7.1 Relative permeability

3.7.2 Complex Permeability

3.1. B-H Loop Shape

The most important characteristics desired for a soft magnetic material are high saturation induction B (or equivalently saturation magnetization *MJ*), high permeability, low coercivity *H,* and low core loss, all of which can be visualized in the *B-H* loop, as can be seen in Fig. 3.1.

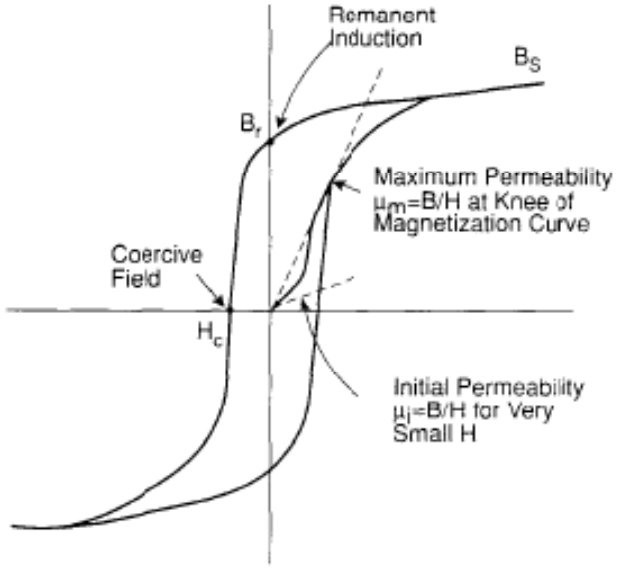

Fig.3.1. Typical *B-H* (hysteresis) loop of a soft magnetic material showing initial magnetization and induction under cyclic excitation, saturation and remanent inductions B_s, and B_r, coercive field H_c, initial permeability μ_i, and maximum permeability μ_{max}

In any magnetic circuit, there is a source of magnetomotive force, either from flowing currents or from permanent magnets, giving rise to magnetic field *H* and magnetic induction *B***.** In a ferromagnetic material,

each magnetic atom carries a substantial magnetic moment which is coupled by quantum mechanical exchange effects to the neighboring moments. Below the Curie temperature T_c, the exchange energy is sufficient to overcome thermal disorder, resulting in a finite spontaneous magnetization. The total magnetization M is just the vector sum of the moments of all individual atoms and $B = \mu_0 H + M$, where μ_0 is the permeability of free space, $4\pi \times 10^{-7}$ H/m in SI units. In a soft magnetic material, M follows H readily, yielding relative permeabilities $\mu = B/\mu_0 H$ in some cases 10^6 or larger. Magnetic materials also exhibit hysteresis, the non-linear, non-local relationship between B and H, which is parametrically displayed as the *B*-*H* loop. Soft and hard magnetic materials have comparable saturation inductions, but are distinguished by their vastly different coercivities: 0.2-100 A/m and 200-2000 kA/m, respectively, for common commercial materials.

3.2 Core *Loss*

The best single measure of evolution of soft magnetic materials is the reduction of core loss. Core losses in metallic magnetic materials are now recognized to stem from the dissipation of the ohmic loss caused by

currents which are induced by changing flux in accordance with Faraday's law. The minimum possible loss per unit volume of a magnetic material is the classical eddy current loss P_{cl}. For a strip material under sinusoidal flux excitation:

$$P_{cl} = (\pi B_{max} f h)^2 / 6\rho \qquad 3.1$$

where B is maximum induction, f is frequency, ρ is electrical resistivity and h is thickness. The classical loss presumes that B changes uniformly through the cross-section of the sample. In practice, the total loss of any real magnetic material is higher than P_{cl},. The discrepancy arises from an inevitable consequence of magnetic domain structure. In other than special circumstances, the magnetic structure of a ferromagnet is characterized by macroscopic regions called magnetic domains. Within each domain, magnetization is essentially uniform in magnitude and direction; domain walls provide the transition between these regions. The magnetization process proceeds at least partially by motion of the walls. As H changes, the dipolar energy $E_d = -\int M.H\, dV$ is decreased by the growth of domains in which M is favorably aligned with H at the expense of anti-aligned domains. Hence, the total magnetization $M = \frac{1}{V} M dV$ increases.

The discontinuous, spatially non-uniform nature of wall motion is responsible for hysteresis and energy dissipation even under quasi-static excitation and for the Barkhausen effect.

3.3 Magnetic Anisotropy

A key factor in our ability to tailor soft magnetic materials for a broad spectrum of applications is an understanding of magnetic anisotropy and how a control by a choice of composition and thermomechanical processing. Magnetic anisotropy is the tendency of the magnetization vector within a piece of magnetic material to be aligned in a particular direction called the easy axis of magnetization. In an actual sample, the net direction of the magnetization is determined by a competition among the dipolar energy Ed and the various sources of anisotropy, principally magnetocrystalline anisotropy, stress anisotropy, induced uniaxial anisotropy, and shape anisotropy.

When a material is magnetized along its easy axis, permeability is high and saturation is easily achieved; in a hard direction, a field $H_k = 2\pi/M_s$, (the anisotropy field) is needed to rotate the magnetization

direction in the presence of an anisotropy energy density *K,* see fig. 3.2. Anisotropy is important even for easy-axis magnetization: in the simplest approximation the initial permeability $\mu_i \propto {}^{1}/_{K}$ while the approach to saturation always involves rotational magnetization of at least some closure domain regions.

In the language of quantum mechanics, each magnetic atom carries both spin (S) and orbital (L) angular momentum. Each of the magnetic electrons' eigenstates has a particular spatial charge distribution which interacts electrostatically with the crystal field produced by the charge cloud surrounding the neighboring atoms. Those magnetic wavefunctions which minimize the electrostatic interaction are energetically favored. The symmetry of the crystal field and the allowed magnetic electron wavefunctions establish the easy axis of magnetization. With uniaxial symmetry the anisotropy has a functional form with leading term $K = K_{u1}\sin^2\theta$, where θ is the angle between *M* and the easy axis. In a cubic

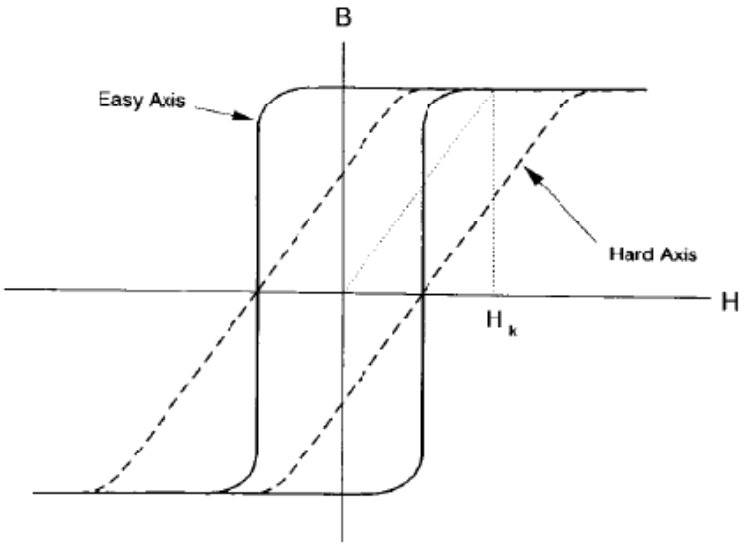

Fig. 3.2. Schematic *B*-*H* loops with magnetization

along the easy and hard axis of magnetization.

system, $K_{u1} = 0$ and a much weaker term $K_1(l^2m^2 + m^2n + n^2l^2)$, where l, m, and n are the direction cosines of *M,* normally dominates. Depending on the sign of K_1, for example either the [001] (α -Fe) or [111] (α -Ni) direction may be the easy axis. The magnitude of the anisotropy energy varies widely. The crystal field acts directly on L but only indirectly on S through spin-orbit coupling $\lambda L.S$.

3.4 Coercivity Field

Coercivity or coercive field, of a ferromagnetic material is the intensity of the applied magnetic field required to reduce the magnetization

of that material to zero after the magnetization of the sample has been driven to saturation. Coercivity is usually measured in O_e or A/m units and is denoted H_C.

Materials with high coercivity are called as hard ferromagnetic materials, and are utilized for permanent magnets. Permanent magnets find application in electric motors, magnetic recording media and magnetic separation. A material with a low coercivity is said to be soft and may be used in microwave devices, magnetic shielding, transformers, or recording heads.

Typically the coercivity of a magnetic material is determined by measurement of the hysteresis loop or magnetization curve. The apparatus used for the measurement is typically a vibrating-sample or alternating-gradient magnetometer. The applied field where the magnetization crosses to zero is the coercivity. If an antiferromagnet is present in the sample, the coercivities measured in increasing and decreasing fields may be unequal as a result of the exchange bias effect.

The coercivity of a material depends on the time scale over which a magnetization curve is measured. The magnetization of a material measured at an applied reversed field which is nominally smaller than the coercivity may, over a long time scale, slowly creep to zero. Creep occurs when reversal of magnetization by domain wall motion is thermally activated and is dominated by magnetic viscosity. The increasing value of coercivity at high frequencies is a serious obstacle to the increase of data rates in high-bandwidth magnetic recording, compounded by the fact that increased storage density typically requires a higher coercivity in the media.

At the coercive field, the vector component of the magnetization of a ferromagnet measured along the applied field direction is zero. There are two primary modes of magnetization reversal: rotation and domain wall motion. When the magnetization of a material reverses by rotation, the magnetization component along the applied field is zero because the vector points in a direction orthogonal to the applied field. When the magnetization reverses by domain wall motion, the net magnetization is small in every vector direction because the moments of all the individual domains sum to

zero. Magnetization curves dominated by rotation and magnetocrystalline anisotropy are found in relatively perfect magnetic materials used in fundamental research. Domain wall motion is a more important reversal mechanism in real engineering materials since defects like grain boundaries and impurities serve as nucleation sites for reversed-magnetization domains. The role of domain walls in determining coercivity is complex since defects may *pin* domain walls in addition to nucleating them.

As with any hysteretic process, the area inside the magnetization curve during one cycle is work that is performed on the magnet. Common dissipative processes in magnetic materials include magnetostriction and domain wall motion. The coercivity is a measure of the degree of magnetic hysteresis and therefore characterizes the lossiness of soft magnetic materials for their common applications.

The *squareness* ($M(H=0)/M_s$) and coercivity are figures of merit for hard magnets although *energy product* (saturation magnetization times coercivity) is most commonly quoted. The 1980s saw the development of rare earth boride magnets with high energy products but undesirably low

Curie temperatures. Since the 1990s new exchange spring hard magnets with high coercivities have been developed.

3.5 Domain wall

In magnetism, a domain wall is an interface separating magnetic domains. It is a transition between different magnetic moments and usually undergoes an angular displacement of 90° or 180°. Domain wall is a gradual reorientation of individual moments across a finite distance. The domain wall thickness depends on the anisotropy of the material, but on average spans across around 100-150 atomic radii.

The energy of a domain wall is simply the difference between the magnetic moments before and after the domain wall was created. This value is usually expressed as energy per unit wall area.

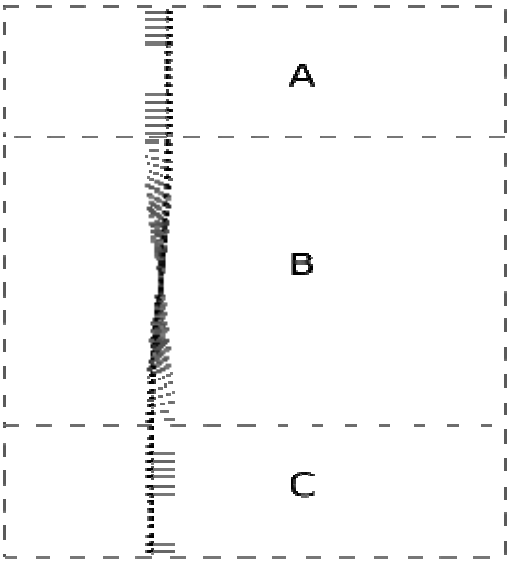

Fig 3.3 Domain wall (B) with gradual re-orientation of the magnetic moments between two 180-degree domains (A) and (C)

The width of the domain wall varies due to the two opposing energies that create it: the Magnetocrystalline anisotropy energy and the exchange energy (J_{ex}), both of which want to be as low as possible so as to be in a more favorable energetic state. The anisotropy energy is lowest when the individual magnetic moments are aligned with the crystal lattice axes thus reducing the width of the domain wall. Whereas the exchange energy is reduced when the magnetic moments are aligned parallel to each other and thus makes the wall thicker, due to the repulsion between them. (Where anti-parallel alignment would bring them closer - working to reduce the wall

thickness.) In the end an equilibrium is reached between the two and the domain wall's width is set as such.

An ideal domain wall would be fully independent of position, however in the actual material, the domain wall get stuck on inclusion sites within the medium, known as crystallographic defects. These include vacancies, interstitials, dislocations, or different atoms, oxides, insulators and even stresses within the crystal. This prevents the formation of domain walls and also inhibits their propagation through the medium. Thus a greater applied magnetic field is required to overcome these sites.

Non-magnetic inclusions in the volume of a ferromagnetic material, or dislocations in crystallographic structure, can cause "pinning" of the domain walls. Such pinning sites cause the domain wall to seat in a local energy minimum and external field is required to "unpin" the domain wall from its pinned position. The act of unpinning will cause sudden movement of the domain wall and sudden change of the volume of both neighbouring domains. This causes Barkhausen noise and in effect it is most likely to be the source of magnetic hysteresis.

3.6 Magnetostriction

Magnetostriction is a property of ferromagnetic materials that causes them to change their shape or dimensions during the process of magnetization. The variation of material's magnetization due to the applied magnetic field changes the magnetostrictive strain until reaching its saturation value, λ. The effect was first identified in 1842 by James Joule when observing a sample of nickel. This effect can cause losses due to frictional heating in susceptible ferromagnetic cores.

The reciprocal effect, the change of the susceptibility of a material when subjected to a mechanical stress, is called the Villari effect. Two other effects are thus related to magnetostriction: the Matteucci effect is the creation of a helical anisotropy of the susceptibility of a magnetostrictive material when subjected to a torque and the Wiedemann effect is the twisting of these materials when a helical magnetic field is applied to them. The **Villari Reversal** is the change in sign of the magnetostriction of iron from positive to negative when exposed to magnetic fields of approximately 40 k

A/m (500 Oe). On magnitude of the magnetostriction, change in volume by applying magnetic field are small: the order of ~10^{-6}.

3.7 Permeability

In electromagnetism, permeability is the measure of the ability of a material to support the formation of a magnetic field within itself. In other words, it is the degree of magnetization that a material obtains in response to an applied magnetic field. Magnetic permeability is typically represented by the Greek letter μ. The term was coined in September 1885 by Oliver Heaviside. The reciprocal of magnetic permeability is magnetic reluctivity.

In SI units, permeability is measured in H/m, or N/A^2. The permeability constant (μ_0), also known as the magnetic constant or the permeability of free space, is a unit of the amount of resistance encountered when forming a magnetic field in vacuum. The magnetic constant is defined to be value of $\mu_0 = 4\pi\times10^{-7} \approx 1.2566370614...\times10^{-6}$ $H\cdot m^{-1}$ or $N\cdot A^{-2}$).

In electromagnetism, the auxiliary magnetic field *H* represents how a magnetic field *B* influences the organization of magnetic dipoles in a given

medium, including dipole migration and magnetic dipole reorientation. Its relation to permeability is

$$B = \mu H \qquad 3.2$$

where the permeability μ is a scalar if the medium is isotropic or a second rank tensor for an anisotropic medium.

In general, permeability is not a constant, as it can vary with the position in the medium, the frequency of the field applied, humidity, temperature, and other parameters. In a nonlinear medium, the permeability can depend on the strength of the magnetic field. Permeability as a function of frequency can take on real or complex values. In ferromagnetic materials, the relationship between *B* and *H* exhibits both non-linearity and hysteresis: *B* is not a single-valued function of *H*, but depends also on the history of the material.

Permeability is the inductance per unit length. In SI units, permeability is measured in H/m = J/(A^2·m) = N/A). The auxiliary magnetic field **H** has dimensions current per unit length and is measured in units of

A/m. The product μH thus has dimensions inductance times current per unit area ($H \cdot A/m^2$). But inductance is magnetic flux per unit current, so the product has dimensions magnetic flux per unit area. This is just the magnetic field B, which is measured in Wb/m^2 ,$V \cdot s/m^2$, T.

B is related to the Lorentz force on a moving charge q:

$$F = q(E + v \times V) \qquad 3.3$$

The charge q is given in C, the velocity v in m/s, so that the force F is in N:

$$qv \times B = C \cdot \frac{m}{s} \cdot \frac{V.s}{m^2} = \frac{C.\left(J/C\right)}{m} = \frac{J}{m} = N \qquad 3.4$$

H is related to the magnetic dipole density. A magnetic dipole is a closed circulation of electric current. The dipole moment has dimensions current times area, units $A \cdot m^2$, and magnitude equal to the current around the loop times the area of the loop. The H field at a distance from a dipole has magnitude proportional to the dipole moment divided by distance cubed, which has dimensions current per unit length.

3.7.1 Relative permeability

Relative permeability, sometimes denoted by the symbol μ_r, is the ratio of the permeability of a specific medium to the permeability of free space given by the magnetic constant $\mu_0 = 4\pi \times 10^{-7}$:

$$\mu_r = \frac{\mu}{\mu_0} \qquad 3.5$$

In terms of relative permeability, the magnetic susceptibility is:

$$\chi_m = \mu_r - 1. \qquad 3.6$$

χ_m, a dimensionless quantity, is sometimes called *volumetric* or *bulk* susceptibility, to distinguish it from χ_p (*magnetic mass* or *specific* susceptibility) and χ_M (*molar* or *molar mass* susceptibility).

3.7.2 Complex Permeability

A useful tool for dealing with high frequency magnetic effects is the complex permeability. While at low frequencies in a linear material the magnetic field and the auxiliary magnetic field are simply proportional to each other through some scalar permeability, at high frequencies these

quantities will react to each other with some lag time. These fields can be written as phasors, such that:

$$H = H_0 e^{j\omega t} \tag{3.7}$$

$$B = B_0 e^{j(\omega t - \delta)} \tag{3.8}$$

where δ is the phase delay of *B* from *H*. Understanding permeability as the ratio of the magnetic field to the auxiliary magnetic field, the ratio of the phasors can be written and simplified as

$$\mu = \frac{B}{H} = \frac{B_0 e^{j(\omega t - \delta)}}{H_0 e^{j\omega t}} = \frac{B_0}{H_0} e^{-j\delta}, \tag{3.9}$$

so that the permeability becomes a complex number. By Euler's formula, the complex permeability can be translated from polar to rectangular form,

$$\mu = \frac{B_0}{H_0}\cos\delta - j\frac{B_0}{H_0}\sin\delta = \mu' - j\mu'' \tag{3.10}$$

The ratio of the imaginary to the real part of the complex permeability is called the loss tangent,

$$\tan\delta = \frac{\mu''}{\mu'} \tag{3.11}$$

which provides a measure of how much power is lost in a material versus how much is stored.

Chapter 4

Result and Discussion

4.1 Resistivity

4.2 Film Structure Characterization

4.3 M-H Loop graph

4.4 Permeability

4.5 Core Loss

4.1 Resistivity

The electrical resistivity was measured by using a conventional four probe method. Figure 4.1 shows the electrical resistivity of $Co_{87}Zr_5Nb_8$ samples with different thickness and argon gas pressure. It is noticeable the ρ are hardly dependent on the deposition gas pressure and film thickness. The resistivity of The $Co_{87}Zr_5Nb_8$ samples has resistivity of ~120 μΩ-cm. This value is much higher than NiFe and CoZrTa [2] which have resistivity value of 20 μΩ-cm, and 100 μΩ-cm, respectively. The electrical resistivity value is very important, that will reduce eddy currents and a ferromagnetic resonance of frequency more that 100 MHz. So that higher value of electrical resistivity is better.

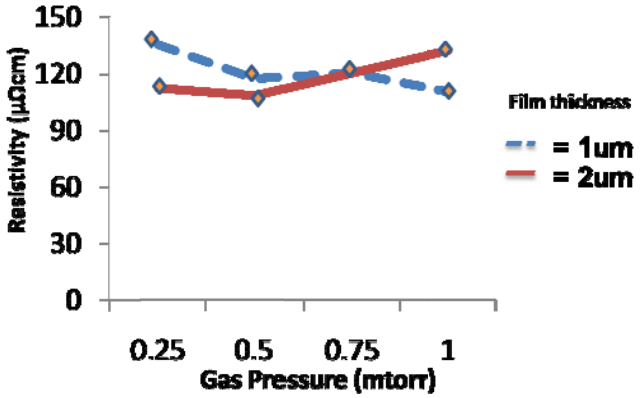

Figure 4.1. Resistivity of $Co_{87}Zr_5Nb_8$ samples with different thickness and argon gas pressure

4.2 Film Structure Characterization

Film texture and surface morphology were observed by using Scanning Electron Microscope (SEM). SEM was also used to measure the film thickness. Figure 4.2 shows cross-sectional SEM image of 1-μm thick $Co_{87}Zr_5Nb_8$ alloy film deposited at 1 mTorr.

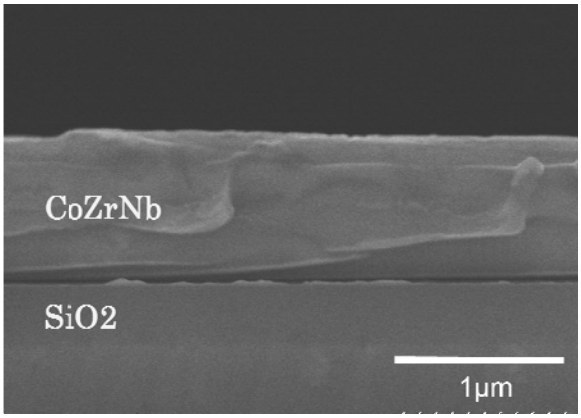

Figure 4.2. Cross-sectional SEM images of 1-μm thick $Co_{87}Zr_5Nb_8$ alloy film deposited at 1 mTorr

A SiO_2 film was chosen as a insulator, that is the same layer structure as the proposed on-chip inductor. Fig. 4.3 shows planar SEM images of $Co_{87}Zr_5Nb_8$ alloy film surface deposited at 0.25 mTorr, 0.5 mTorr, 0.75mTorr, and 1 mTorr. All the surface morphologies at these gas pressure conditions are quite the same.

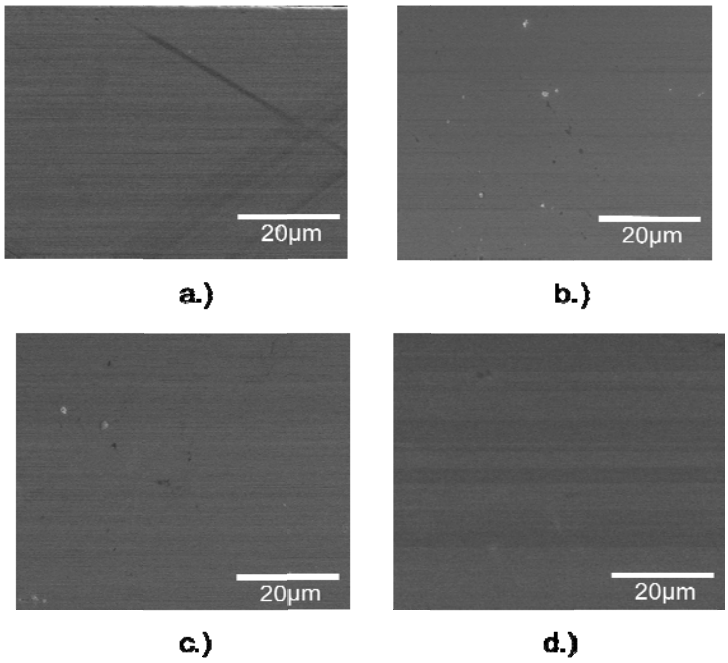

Figure 4.3 SEM images of $Co_{87}Zr_5Nb_8$ alloy film surface deposited at a.) 0.25 mTorr, b.) 0.5 mTorr, c.) 0.75mTorr, and d.) 1 mTorr.

4.3 M-H Loop graph

M-H magnetic hysteresis loops were measured of the easy and hard axis orientations to study the saturation magnetization and hysteresis losses. The 0.5-µm thick $Co_{87}Zr_5Nb_8$ alloy film deposited at 1 mTorr exhibits a relatively high saturation magnetization of ~1200 emu/cm^3 $\cong$ 15.1 kG and low initial coercivity of 1.8 Oe that minimizes hysteresis losses (see Fig 4.4). A high coercivity will negatively impact the small signal permeability. From fig. 4.4 can be seen that isotropy field for this sample is 18 Oe.

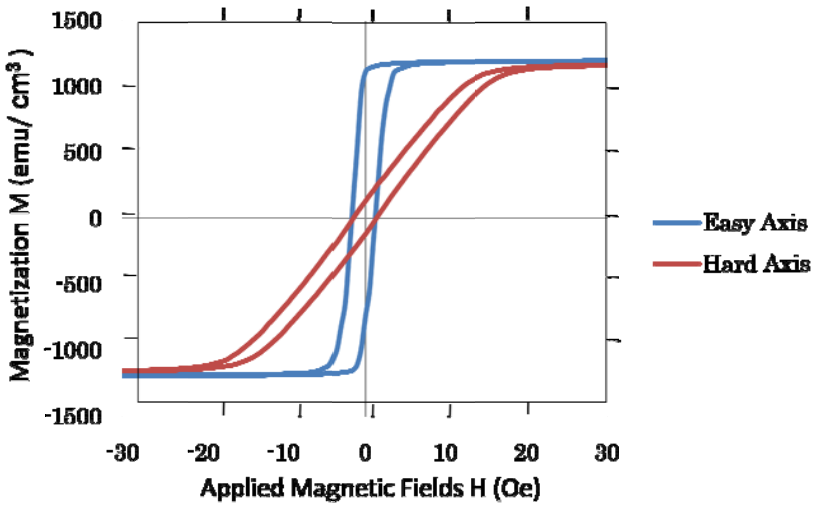

Figure 4.4. Magnetic hysteresis loops of 0.5-μm thick $Co_{87}Zr_5Nb_8$ alloy film deposited at 1 mTorr

Saturation magnetization decreased to 1000 emu/cm^3 when the film thickness increased to 1-μm, as can be seen in fig 4.5. Coercivity value and isotropy field are 1.9 Oe, and 16 Oe, respectifely. When the film thickness increased to 2-μm, saturation magnetization further decreased to 909 emu/cm^3 (see fig 4.6). The coercivity value and isotropy field for this film are 1.8 Oe, and 17 Oe, respectifely. As already explained in Chapter 3, lower coercivity and higher isotrophy field value are better. From these results, it can be summarized that coercivity and isotrophy field are not dependent on the film thickness.

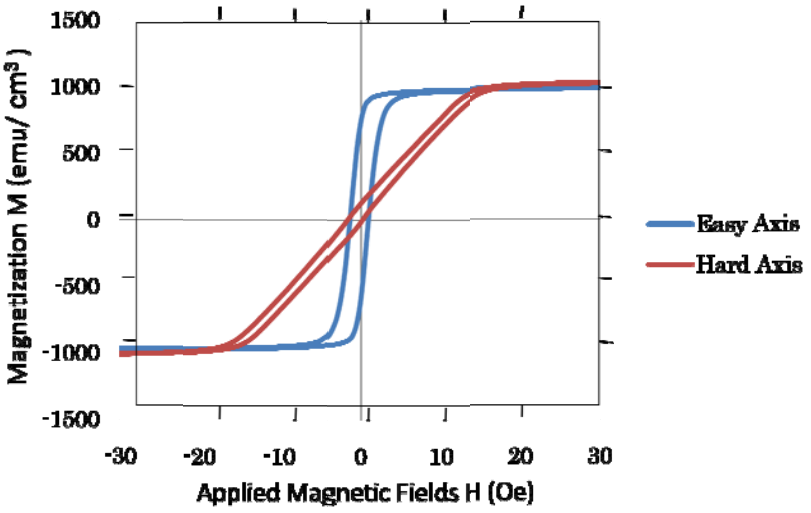

Figure 4.5. Magnetic hysteresis loops of 1-µm thick $Co_{87}Zr_5Nb_8$ alloy film deposited at 1 mTorr

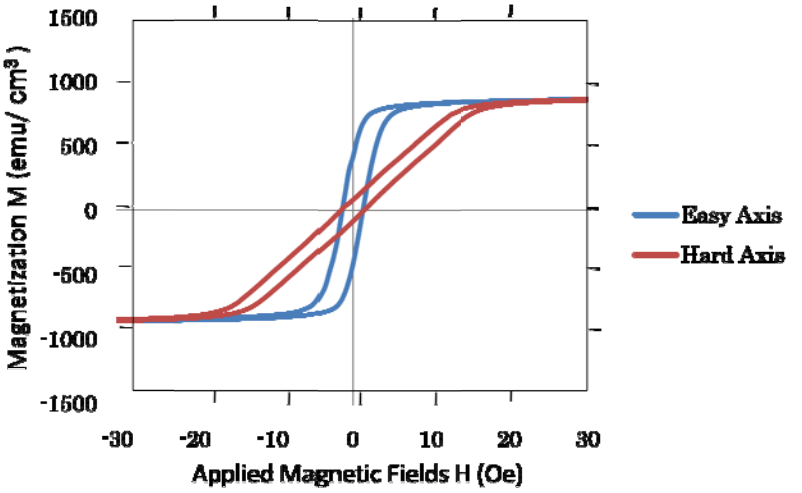

Figure 4.6 Magnetic hysteresis loops of 2-µm thick $Co_{87}Zr_5Nb_8$ alloy film deposited at 1 mTorr

The magnetic properties of $Co_{87}Zr_5Nb_8$ alloy films were summarized in Table 4.1. It is noticeable the value of Hc, Hk, are hardly dependent on the deposition gas pressure and film thickness.

Table 4.1. Properties of $Co_{87}Zr_5Nb_8$

Thickness (μm)	Pressure during deposition (mTorr)	Ms (emu/cm^3)	Hce (Oe)	Hch (Oe)	Hk (Oe)
1.0	0.25	812	2.0	1.8	17
1.0	0.50	925	4.5	2.0	18
1.0	0.75	894	3.5	1.5	16
1.0	1.0	1000	2.4	1.9	16
2.0	0.25	816	3.3	1.6	16
2.0	0.50	925	4.5	1.8	17
2.0	0.75	1000	1.6	1.5	18
2.0	1.0	909	1.8	1.9	17

4.3 Permeability

The small signal permeability as a function of frequency up to 500 MHz was measured, as can be seen in Fig 4.7. As the film thicknesses increases, the real component of the permeability decreases and the

imaginary component increases because of the skin effect and eddy currents. The skin effect reduces the effective permeability of the medium. In addition, the effects of eddy currents start to dominate thereby reducing the effective complex permeability μ as:

$$\mu = \mu_i \frac{2\delta}{(1+j)\mathrm{d}} tanh \frac{(1+j)\mathrm{d}}{2\delta} \qquad 4.1$$

where the thickness of the magnetic film is d and dc permeability is μ_i.

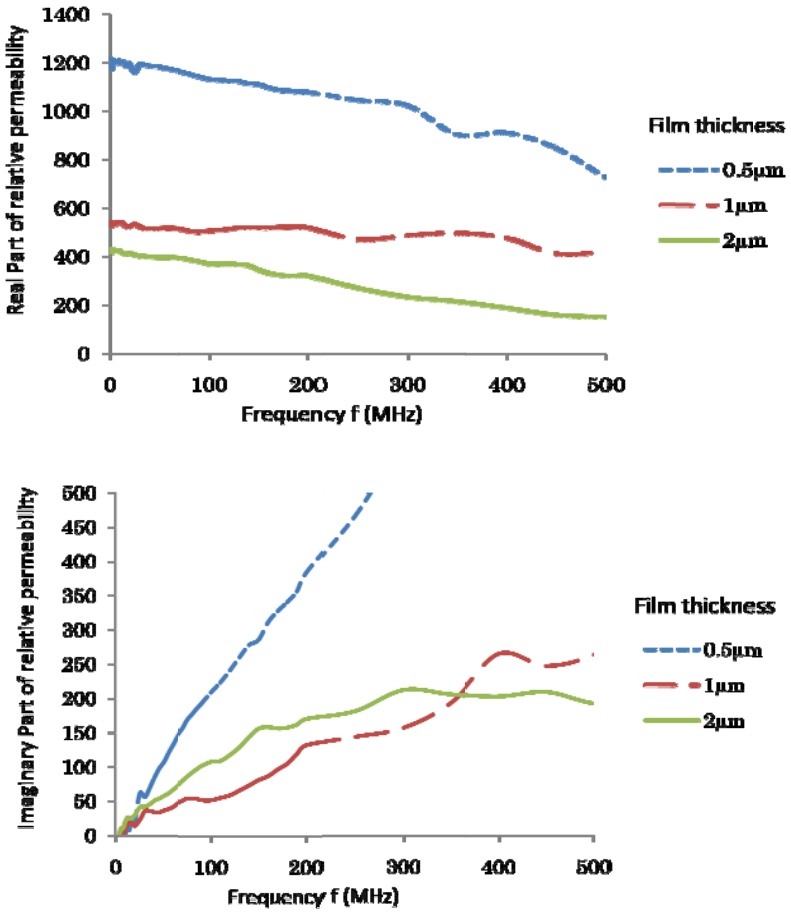

Figure 4.7 Frequency dependences of real and imaginary components of the relative permeability

4.4 Core Loss

The losses can be evaluated using the imaginary permeability μ'' in the equation:

$$\tan \delta_{\mu} = \mu'' / \mu' \qquad 4.2$$

As the film thickness increases, the losses increase at higher frequencies (see figure 4.8). For high frequency applications, film alloy thicker than 1-μm is not suitable because of high core loss.

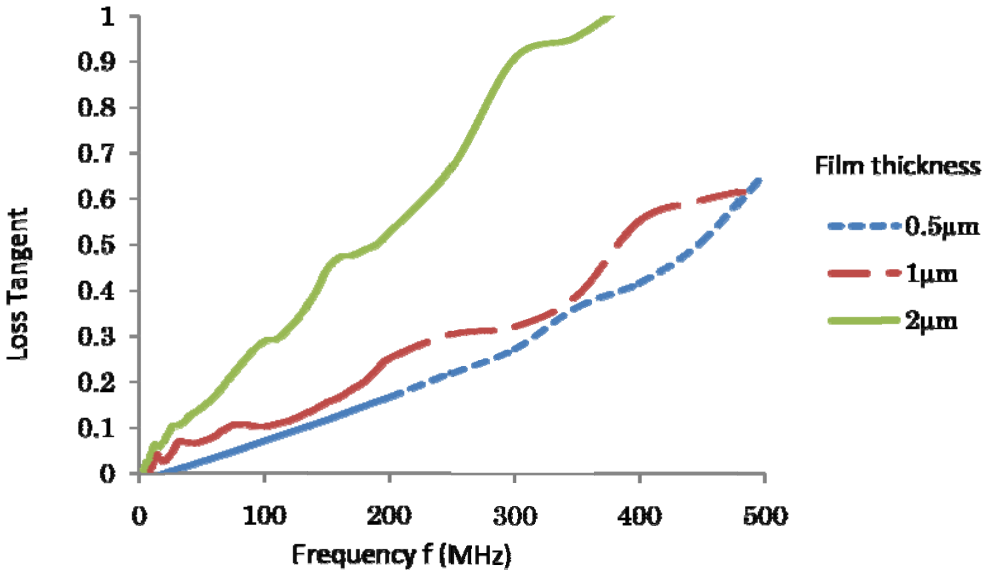

Figure 4.8 The loss tangent versus frequency of $Co_{87}Zr_5Nb_8$

Chapter 5
Conclusions of This Study

5.1 Properties of $Co_{87}Zr_5Nb_8$

5.2 Future Works

5.1 Properties of $Co_{87}Zr_5Nb_8$

Electrical and magnetic properties of the amorphous $Co_{87}Zr_5Nb_8$ films were examined. The $Co_{87}Zr_5Nb_8$ alloy film deposited at 1 mTorr exhibits a relatively high saturation magnetization of ~1200 emu/cm^3 ≅ 15.1 kG and low initial coercivity of 1.8 Oe that minimizes hysteresis losses. Coercivity (~2 Oe), anisotropy field (~17 Oe), resistivity (~120 Ωcm) did not depend on the deposition conditions and thickness up to 2 μm. $Co_{87}Zr_5Nb_8$ has ferromagnetic resonance of 1.3 GHz. The 0.5-μm thick $Co_{87}Zr_5Nb_8$ alloy film deposited at 1 mTorr exhibits ~1200 real part permeability up to 500 MHz. Core loss performance of $Co_{87}Zr_5Nb_8$ alloy film thinner than 1μm shows good properties up to 500 MHz. The current results show that $Co_{87}Zr_5Nb_8$ is a suitable magnetic material for the proposed on-chip inductor with switching frequency range up to 500 MHz.

$Co_{87}Zr_5Nb_8$ is rated as good soft magnetic alloy for the proposed on-chip inductors because of its good combination of magnetic properties. High saturation magnetization and low coercivity of the magnetic material

are important because they will limit the maximum current density and determine the hysteretic losses.

5.2 Future works

In the next step, fabrication of on-chip inductor will be conducted using $Co_{87}Zr_5Nb_8$ as magnetic film layer. Consider to the research result, 1-μm, 0.5-μm or thinner $Co_{87}Zr_5Nb_8$ film alloys will be suited. There are various ways to integrate magnetic materials into inductor structures, as shown in Figure 5.1. In Figure 5.1, the sandwich structure is the most efficient method to reduce the magnetic energy leak and to increase the inductor performance compared with other ways. In the next step, A study of $Co_{87}Zr_5Nb_8$ magnetic film layer insertion into on-chip inductor sandwich structure will be conducted.

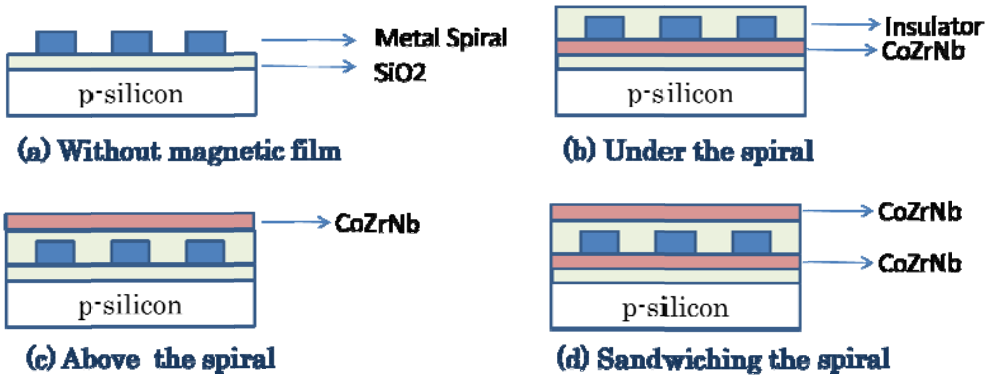

Fig 5.1 various way to integrate magnetic film into on-chip inductor structure.

References

[1] D. S. Gardner, G. Schrom, P. Hazucha, F. Paillet, T. Karnik and S. Borkaret, *IEEE Trans. Magn.,* vol.43, no.6, pp.2615-2617, June (2007).

[2] D. S. Gardner, G. Schrom, P. Hazucha, F. Paillet, T. Karnik, S. Borkaret, R. Hallstein, T. Dambrauskas, C. Hill, C. Linde, W. Worwag, R. Baresel, and S. Muthukumar, *J. Appl.Phys.,* 103, 07E927 (2008).

[3] M. Yamaguchi, *J. Appl. Phys.*, vol. 85, no. 11, pp. 7919-7922, (1999).

[4] S. S. Mohan, M. Hershenson, S.P. Boyd, and T. H. Lee, *IEEE J. Solid State Circuits,* vol. 34, no. 10, pp. 1419-1424, Oct (1999).

[5] G. E. Fish, *IEEE. Vol. 78, no. 6,* June (1990)

[6] Ito T. et. al., J. Magn. Soc. Japan, 28, 401, (2004)

[7] J. Michel, Y. Lamy, A. Royet, and B. Viala*,* in *Proc. Int. Magn.*, p. 57, (2007).

[8] A. Crawford, D. S. Gardner, and S. Wang*, IEEE Trans. Magn.*, vol. 40, no. 4, pp. 2017–2019, Jul. (2004).

[9] M.E. McHenry, M. A. Willard, D. E. Laughlin. Progress in Materials Science, vol. 44, pp. 291-433, (1999).

[10] J. Salvia, J. A. Bain, and C. P. Yue*, Proc. IEEE IEDM*, pp. 943–946, (2005).

[11] M. Yamaguchi, M. Baba, and K. I. Arai*, T. Microwave Theory*, vol. 49, no. 12, pp. 2331–2335, (2001).

[12] V. Korenivski, R. B. Van Dover. IEEE Trans. Mag., 34., pp. 1375, (1998).

[13] T. Sato, H. Tomita, A. Sawabe, T. Inoue, T. Mizoguchi, M. Sahashi: *IEEE Trans. Mag.,* vol. 30, pp. 217, (1994).

[14] M. H. Park, Y. K. Hong, S. H. Gee, M. L. Mottern, T. W. Jang, S. Burkett, *J. Appl. Phys.,* vol. 91, pp. 7218, (2002).

[15] N. X. Sun, S. X. Wang, *J. Appl. Phys.,* vol. 92, pp. 1477, (2002).

Acknowledgments

I would like to thank my academic supervisor Professor Nobuyuki Sugii, and Professor Hiroshi Iwai for their excellent guidance and continuous encouragement, as well as financial support of the project. I am great thanks to Associate Professor Yoshitaka Kitamoto from Department of Innovative and Engineered Material for his supervision on my research. I am deeply thanks to Assistant Professor Kuniyuki Kakushima for his continuous supports.

I would also like to express gratitude to Professor Takeo Hattori, Professor Kenji Natori, Professor Akira Nishiyama, Professor Kazuo Tsutsui, and Associate Professor Parhat Ahmet for for many useful advices. Thanks to Prof. Shigeki Nakagawa from graduate school of science and engineering Tokyo Institute of Technology, and Prof. Nobuhiro Matsushita from interdisciplinary graduate school of science and engineering, Tokyo Institute of Technology for their support.

Thanks to all Iwai Laboratory member for their kind friendship. I would like to express sincere gratitude to laboratory secretaries, Ms. A. Matsumoto, Ms. M. Karakawa, and Ms. M. Nishizawa. Thanks to Indonesia Ministry of Education for providing DIKTI scholarship.

Finally, I would like to thank my family for their endless love and support.

July 2010

Mokh. Sholihul Hadi